Vol 18 No 9, September 2009
1674-1056/2009/18(09)/3995-05

Chinese Physics B

© 2009 Chin. Phys. Soc.
and IOP Publishing Ltd

A novel structure of a high current gain 4H-SiC BJT with a buried layer in the base

Zhang You-Run(张有润)†, Zhang Bo(张 波),
Li Zhao-Ji(李肇基), Deng Xiao-Chuan(邓小川), and Liu Xi-Ling(刘曦麟)

State Key Laboratory of Electronic Thin Films and Integrated Devices, University of Electronic Science and Technology of China, Chengdu 610054, *China*

(Received 10 November 2008; revised manuscript received 20 January 2009)

In this paper, a new structure of a 4H-SiC bipolar junction transistor (BJT) with a buried layer (BL) in the base is presented. The current gain shows an approximately 100% increase compared with that of the conventional structure. This is attributed to the creation of a built-in electric field for the minority carriers to transport in the base which is explained based on 2D device simulations. The optimized design of the buried layer region is also considered by numeric simulations.

Keywords: 4H-SiC, bipolar junction transistor (BJT), buried layer, current gain
PACC: 7340L, 7280

1. Introduction

Silicon carbide (SiC) is a very attractive material for high voltage, high temperature and high power applications due to its wide bandgap, high breakdown field, and high thermal conductivity. The 4H-SiC bipolar junction transistor (BJT) is a promising switching device, and considerable progress has been made in recent years.[1−4] It is an intrinsically normally-off device, has no gate oxide problem, and conducts high current at a low forward voltage. However, a disadvantage with the BJT is that it requires a continuous base current for control. Therefore, improving the current gain of the 4H-SiC BJT is extremely important, as it determines the driving loss of the transistor. However, the 4H-SiC BJT reported in the literature exhibits a low current gain usually in a range of 10–40. Many studies have reported that the current gain of the 4H-SiC BJT can be increased by optimizing the emitter/base geometry,[5] surface passivation,[6] ion implantation,[7] as well as employing double base epilayers.[8] Because most studies have focused on improving the conventional structure, there has not been a new structure that can increase current gain effectively.

In the present paper, for the first time, we report a novel 4H-SiC NPN BJT structure with high current gain. An n-type buried layer is used in the base to eliminate the drawback of low current gain. The collector current can be significantly improved, thus enhancing the current gain up to approximately 100%, which is due to the creation of a built-in electric field for the minority carriers to transport in the base region. By a 2D simulator ATLAS, current gain enhancement does take place in 4H-SiC BL-BJT compared with the experimental conventional structure.[1]

2. Device structure and physical models

Simplified cross-sections of conventional and 4H-SiC BL-BJTs are shown in Fig.1. In the 4H-SiC BL-BJT, there is an n-type layer buried in the p-type base, which is distinguished from the conventional structure. $L_{\rm b}$, $T_{\rm b}$ and $N_{\rm b}$ are the length, thickness and doping concentration of the buried layer respectively. All devices in this study have $N_{\rm b}$ of 5×10^{17} cm^{-3}. A temperature of 300 K is employed as default in the simulations.

The 2D numerical device characteristics are realized with Atlas from Silvaco. In addition to the basic Poisson and drift/diffusion equations, different physical models used simultaneously in Silvaco are Shockley–Read–Hall (SRH) for generation and recombination, bandgap narrowing (BGN) for bandgap narrowing, the Caughey–Thomas model for mobility and finally, incomplete for incomplete ionization of dopants.

†E-mail: yrzhang@uestc.edu.cn

It is worth noting that in the mobility models the carrier velocity saturation, the carrier–carrier scattering (with high doping levels), the carrier diffusion at interface and the vertical electric field influence may be taken into account.[9−11]

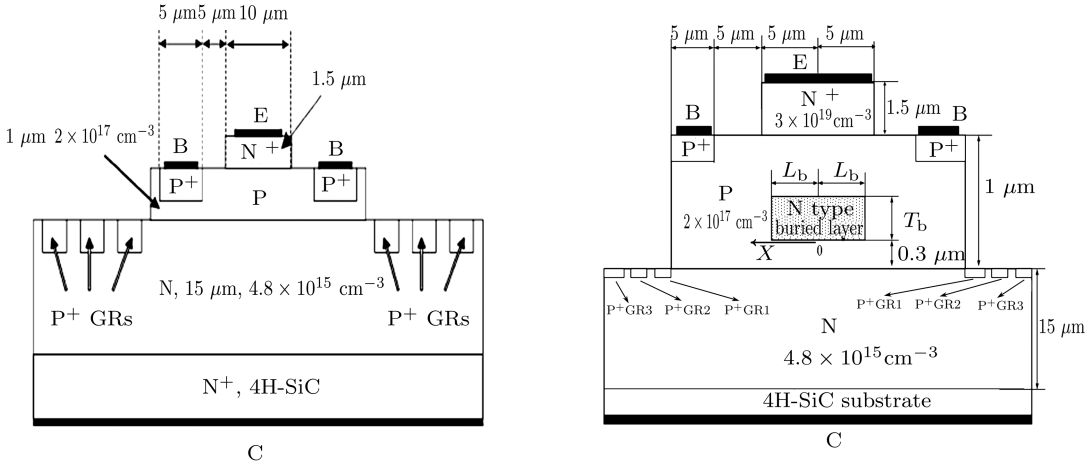


Fig.1. Schematic cross-sections of (a) conventional 4H-SiC BJT and (b) proposed 4H-SiC BJT with a buried layer in the base.

2.1. Bandgap narrowing model

A high concentration of free carriers in a semiconductor can cause a significant reduction in bandgap. At high doping levels, carrier–carrier interaction, carrier–impurity interaction and overlap of the electron wave functions are not negligible. These bandgap narrowing effects are taken into account in band edge displacements that can be described as[12]

$$\begin{aligned}\Delta E_{\mathrm{C}} &= (-1.5\times10^{-2})\left(\frac{N_{\mathrm{D}}^{+}}{10^{18}}\right)^{1/3} \\ &\quad +(-2.93\times10^{-3})\left(\frac{N_{\mathrm{D}}^{+}}{10^{18}}\right)^{1/2}, \\ \Delta E_{\mathrm{V}} &= (1.9\times10^{-2})\left(\frac{N_{\mathrm{D}}^{+}}{10^{18}}\right)^{1/4} \\ &\quad +(8.74\times10^{-3})\left(\frac{N_{\mathrm{D}}^{+}}{10^{18}}\right)^{1/2}. \end{aligned} \tag{1}$$

Bandgap narrowing has an important effect in bipolar transistors by increasing the minority carrier concentration in the emitter, thus reducing the emitter efficiency.

2.2. Mobility models

The Caughey–Thomas model[13] is commonly used for describing the carrier mobility of SiC. The mobilities of electron and hole at low electric fields are both dependent on the doping level and temperature, and they are given respectively by

$$\begin{aligned}\mu_{\mathrm{n}}(\mathrm{cm}^2/\mathrm{V}\cdot\mathrm{s}) &= \frac{947\times(T/300)^{-2}}{1+[N_{\mathrm{i}}/(1.94\times10^{17})]^{0.61}}, \\ \mu_{\mathrm{p}}(\mathrm{cm}^2/\mathrm{V}\cdot\mathrm{s}) &= 15.9+\frac{124\times(T/300)^{-2}}{1+[N_{\mathrm{i}}/(1.76\times10^{19})]^{0.34}}, \end{aligned} \tag{2}$$

where N_{i} denotes the total concentration of ionized impurities.

At high electric fields, the carrier drift velocity saturates due to an increase in optical phonon scattering and reaches saturation velocity. The mobilities of electron and hole at high electric fields can be expressed respectively as

$$\begin{aligned}\mu_{\mathrm{n}}(\mathrm{cm}^2/(\mathrm{V}\cdot\mathrm{s})) &= \frac{\mu_{\mathrm{n0}}}{\left[1+\left[\dfrac{\mu_{\mathrm{n0}}E}{V_{\mathrm{sat}}}\right]^2\right]^{0.5}}, \\ \mu_{\mathrm{p}}(\mathrm{cm}^2/(\mathrm{V}\cdot\mathrm{s})) &= \frac{\mu_{\mathrm{p0}}}{1+\left[\dfrac{\mu_{\mathrm{n0}}E}{V_{\mathrm{sat}}}\right]}, \end{aligned} \tag{3}$$

where μ_{n0} and μ_{p0} are the mobilities of electron and hole at low electric fields respectively. V_{sat} is the saturation velocity with a value of 2×10^7 cm/s for 4H-SiC.

2.3. Carrier lifetime model

The SRH lifetime depends on the doping concentration and the temperature. The doping dependence

of the SRH lifetime is modelled with the Scharfetter relation,[13] and the temperature dependence is modelled by a power law.[13] Thus, the electron lifetime is expressed as follows:

$$\tau_{\rm n} = \frac{\tau_{\rm max,n}\left(\dfrac{T}{300}\right)^{1.72}}{1+\left(\dfrac{N_{\rm i}}{3\times 10^{17}}\right)^{0.3}}, \tag{4}$$

where T is the lattice temperature in K, $N_{\rm i}$ is the total concentration of ionized impurities, and $\tau_{\rm max,n}$ is the electron lifetime in the material without impurities at 300 K. The parameter α is cited from Ref.[14] and the parameter γ is taken from Ref.[15]. The relation $\tau_{\rm n} = 5\tau_{\rm p}$ is used in the simulation.

2.4. Incomplete ionization model

The donor and the acceptor energy levels ($E_{\rm D}$ and $E_{\rm A}$) in SiC are deeper than the thermal energy at room temperature, so the dopants in SiC are not fully ionized even above room temperature.[16] The ionized concentration for donors ($N_{\rm D}^{+}$) and acceptors ($N_{\rm A}^{+}$) are given by

$$N_{\rm D}^{+} = \frac{N_{\rm D}}{1+g_{\rm c}\exp\left[\dfrac{E_{\rm Fn}-E_{\rm D}}{kT}\right]}, \tag{5}$$

$$N_{\rm A}^{+} = \frac{N_{\rm A}}{1+g_{\rm v}\exp\left[\dfrac{E_{\rm Fp}-E_{\rm A}}{kT}\right]}, \tag{6}$$

where $N_{\rm D}$ and $N_{\rm A}$ are donor and acceptor concentrations of impurities added to the semiconductor crystal. $E_{\rm Fn}$ and $E_{\rm Fp}$ are the quasi-Fermi levels, respectively. Due to the lack of specific information for SiC, the donor energy level degeneracy factor $g_{\rm c}$ and acceptor energy level degeneracy factor $g_{\rm v}$ are usually assumed to have the same values as those in Si. For energy levels of the nitrogen donor in 4H-SiC, a dopant ionization energy $E_{\rm Fn} - E_{\rm D} = 42$ meV and $g_{\rm c} = 2$ can be used. p-type doping can be achieved with Al acceptors with ionization energy $E_{\rm Fp} - E_{\rm A} = 191$ meV and $g_{\rm v} = 4$.

3. Results and discussion

In order to demonstrate the 4H-SiC BL-BJT effect, we first implement the experimental 4H-SiC BJT in ATLAS as shown in Fig.1(a). Figure 2 shows the simulated and experimental collector current–voltage ($I_{\rm C}$–$V_{\rm CE}$) characteristics under the base current ($I_{\rm B}$) varying from 200 to 800 mA in steps of 200 mA. It should be noted that the simulated results of the conventional 4H-SiC BJT are in good agreement with the experimental data.

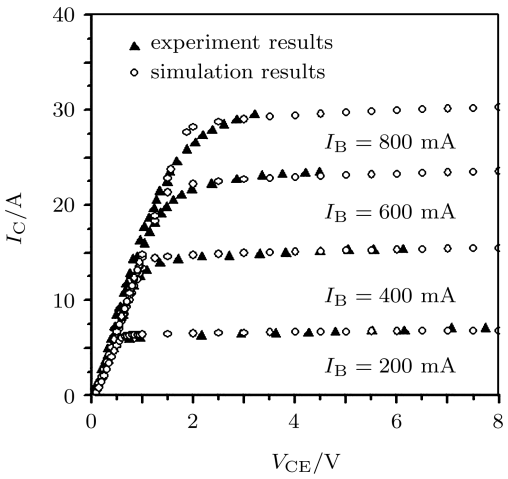


Fig.2. I–V characteristics for the conventional structure of a 4H-SiC BJT.

Figure 3 shows a comparison of the I–V characteristic of the 4H-SiC BJT between the cases with and without buried layers. The results show that the current driving capability of BL-BJT is high compared with that of the conventional structure. The current gain comparison in Fig.4 shows that the BL-BJT ($L_{\rm b} = 5$ μm) exhibits almost double that of the conventional structure. As can be observed from Fig.4, it is represented at moderate current levels that current gain is approximately constant. Compared with the conventional structure, the BL-BJT ($L_{\rm b} = 2$–6 μm) has a wide current application.

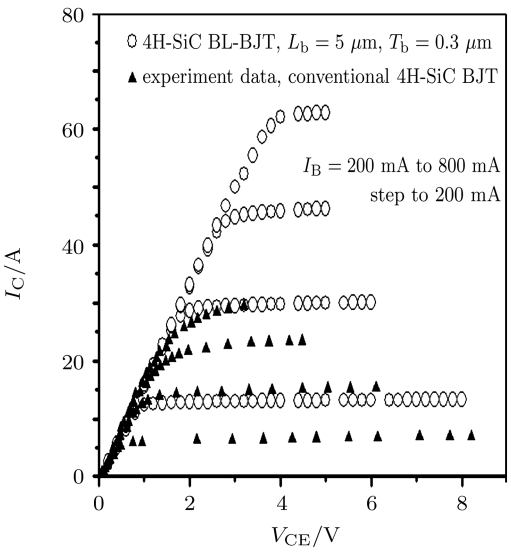


Fig.3. Comparisons of I–V characteristic of the 4H-SiC BJT between the cases with and without buried layers.

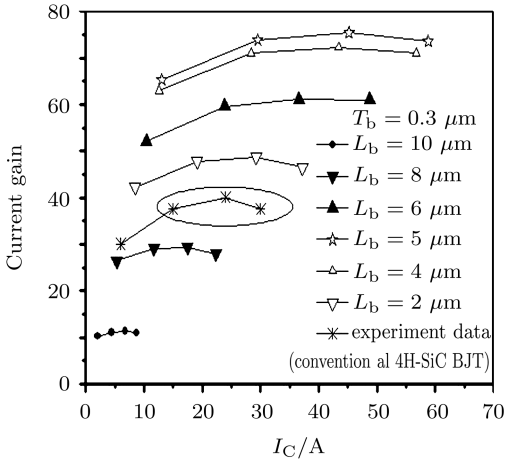


Fig.4. Curves for current gain versus collector current for different lengths of BL.

Figure 5 demonstrates the effect of current density on the distance of the buried layer underside. The x-axis is set on Fig.1(b). The current density with the buried layer approximately doubles at the peak which is responsible for the creation of a built-in electric field for the minority carriers to transport in the base region as compared with that of the conventional structure. The injected electrons from the emitter pass through the base quickly thus reducing base recombination. The effect of current crowding at the edge of the emitter ($x = 5$ μm) can also be observed. As a function of the electric field of the buried layer, the current crowding effect is even more obvious than that of the convention structure.

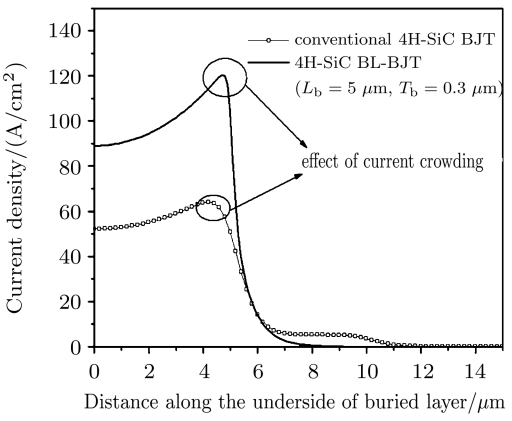


Fig.5. Curves for current density versus distance along the underside of the buried layer.

Figure 6 shows the dependence of maximal current gain on the length of the buried layer with different thicknesses. The values of maximal current gain increase when L_b increases from 2 to 5 μm, and then it decreases sharply when L_b increases from 5 to 10 μm. The simulation results are explained below.

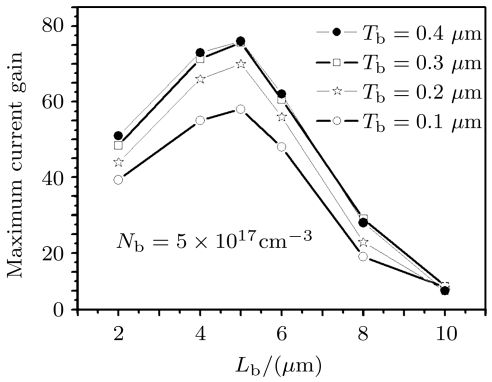


Fig.6. Curves for maximal current gain versus length of buried layer with different thicknesses of buried layer.

Until now, some work has been done to study the mechanisms related to the current gain. The factors limiting the current gain of 4H-SiC BJTs are found to be the bulk carrier recombination in the device base and the emitter injection efficiency. At the same time, in such a wide band gap semiconductor material as SiC, the recombination in the space charge region (SCR) may substantially affect the amplifying properties of BJTs.[17,18] Therefore, in the theoretical analysis the following factors must be taken into account: 1) recombination in the emitter–base space charge region (SCR), 2) effect of the emitter current crowding, and 3) electron mobility decreasing due to the carrier scattering effect.

Common emitter current gain (β) can be expressed as follows:

$$\begin{aligned}
&\beta^{-1} = \beta_{\mathrm{rB}}^{-1} + \beta_{\mathrm{rSCR}}^{-1} + \beta_{\mathrm{E}}^{-1},\\
&\beta_{\mathrm{rB}}^{-1} = \frac{1}{2}\left[\frac{W_{\mathrm{B}}}{L_{\mathrm{nB}}}\right]^2 = \frac{\tau_{\mathrm{b}}}{\tau_{\mathrm{n}}} = \frac{W_{\mathrm{B}}}{\mu_{\mathrm{nB}}|E|\cdot\tau_{\mathrm{n}}},\\
&\beta_{\mathrm{rSCR}}^{-1} = \frac{N_{\mathrm{AB}} W_{\mathrm{B}} W_{\mathrm{BE}}}{2 D_{\mathrm{nB}} \tau_{\mathrm{a}} n_{\mathrm{i}} \mathrm{e}^{qV_{\mathrm{BE}}/2kT}},\\
&\beta_{\mathrm{E}}^{-1} = 1 - \gamma = \frac{D_{\mathrm{pE}}}{D_{\mathrm{nB}}}\frac{W_{\mathrm{B}}}{L_{\mathrm{pE}}}\frac{N_{\mathrm{AB}}}{N_{\mathrm{DE}}},
\end{aligned} \tag{7}$$

where β_{rB}^{-1} is the factor of the recombination in neutral bulk of the base; $\beta_{\mathrm{rSCR}}^{-1}$ is the factor of the recombination in the emitter–base space charge region; γ is the emitter injection efficiency; L_{nB} is the electron diffusion length in the base; N_{AB} and N_{DE} are the acceptor concentration of base and the donor concentration of emitter respectively; D_{nB} and D_{pE} are the electron diffusion constant in the base and the hole diffusion constant in the emitter respectively; W_{B} is the base width; τ_{a} is the ambipolar lifetime ($\tau_{\mathrm{a}} = \tau_{\mathrm{n}} + \tau_{\mathrm{p}}$); τ_{b} is the time of minority carrier transport in the base; W_{BE} is the base–emitter space charge width; μ_{nB} is

the electron mobility in the base; E is the electric field for electrons to transport in the base.

Considering the buried layer in the device base, maximal current gain increases sharply as the length of buried layer increases from 2 to 5 μm. This is attributed to the reducing of factors β_{rB}^{-1} and $\beta_{\mathrm{rSCR}}^{-1}$. Firstly, the buried layer induces a new built-in electric field, thus reducing the time of electron transport τ_{b}. When the buried layer is close to the edge of the emitter which is the location of current crowding, τ_{b} decreases obviously. So the factor β_{rB}^{-1} decreases. Furthermore, the emitter–base space charge region W_{BE} shrinks gradually with the buried layer length increasing from 2 to 5 μm because of the buried layer weakening the electric field of the emitter–base space charge region. So the factor $\beta_{\mathrm{rSCR}}^{-1}$ is decreasing.

As L_{b} increases from 5 to 10 μm, maximal current gain decreases sharply. This is due to two factors: one is that the terminal edge of the buried layer is far from the point of emitter current crowding with L_{b} increasing, the other is that a high level of electron assembled nearby the buried layer leads to a reduction in electron mobility ($\propto D_{\mathrm{nB}}$) due to the mass carrier scattering effect. Therefore, β decreases sharply because of β_{rB}^{-1}, $\beta_{\mathrm{rSCR}}^{-1}$ and β_{E}^{-1} increasing.

Figure 6 also shows the dependence of current gain and the thickness of the buried layer. The maximal current gain increases as T_{b} increases from 0.1 to 0.3 μm and is almost equal to 0.4 μm. This is because the depletion region of the buried layer edge is enhanced with T_{b} increasing. At the same time, simulation results are not sensitive to the BL concentration. Therefore for a given BL concentration (N_{b} of 5×10^{17} cm^{-3}), L_{b} of 5 μm and T_{b} of 0.3 μm are the optimal values.

4. Conclusion

In this paper a new design of a high current gain 4H-SiC BJT with a buried layer in the base is proposed for the first time. The current gain of the 4H-SiC BL-BJTS shows an approximately 100% increase compared with that of the conventional structure. The current gain enhancement is due to the creation of a built-in electric field in the base region helping the injected electrons from the emitter pass through the base quickly, thereby reducing the base recombination. Finally L_{b} of 5 μm and T_{b} of 0.3 μm are the optimal values in simulation. The high current gain obtained for the proposed structure results in low driving losses, thus making this device more useful for high voltage applications.

References

[1] Krishnaswami S, Agarwal A, Ryu S H, Capell C, Richmond J, Palmour J, Balachandran S, Chow T P, Bayne S, Geil B, Jones K and Scozzie C 2005 *Electron Device Lett.* **26** 175

[2] Balachandran S, Chow T P, Agarwal A, scozzie C and Jones K A 2005 *Electron Device Lett.* **26** 470

[3] Ivanov P A, Levinshtein M E, Agarwal A K, Krishnaswami S and Palmour J W 2006 *Electron Devices* **53** 1245

[4] Zhang J H, Li X Q, Alexandrov P, Fursin L, Wang X H and Zhao J H 2008 *Electron Devices* **55** 1899

[5] Domeij M, Lee H S, Danielsson E, Zetterling C M, Ostling M and Schoner A 2005 *Electron Device Lett.* **26** 743

[6] Zhang J, Luo Y, Alexandrov P, Fursin L and Zhao J H 2003 *Electron Device Lett.* **24** 327

[7] Huang C F and Cooper J A 2003 *Electron Device Lett.* **24** 396

[8] Zhang J H, Li X Q, Alexandrov P, Burke T and Zhao J H 2008 *Electron Device Lett.* **29** 471

[9] Deng X C, Zhang B and Li Z J 2007 *Semiconductor Science and Technology* **22** 1339

[10] Deng X C, Zhang B, Li Z J and Chen Z L 2007 *Semiconductor Science and Technology* **22** 701

[11] Zhang J P, Zhang B and Li Z J 2008 *Microelectronic Engineering* **85** 89

[12] Lindefelt U 1998 *J. Appl. Phys.* **84** 2628

[13] Device Simulator Atlas. 2008 Atlas User's Manual. Silvaco International

[14] Kordina O and Bergman J P 1996 *Appl. Phys. Lett.* **69** 679

[15] Ruff M, Mitlehner H and Helbig R 1994 *Electron Dev.* **41** 1040

[16] Capano M A, Santhakumar R, Venugopal R, Melloch M R and Cooper J A 2000 *J. Electronic Materials* **29** 210

[17] Ivanov Pavel A, Levinshtein M E, Rumyantsev S L, Ryu S H, Agarwal A K and Palmour J W 2002 *Solid-State Electronics* **46** 567

[18] Luo J S and Yan B P 1996 *Chin. Phys.* **5** 923